

Long-term biogenic soil mixing and transport in a hilly, loess-mantled landscape: Blue Mountains of southeastern Washington

S.C. Walther ^{a,*}, J.J. Roering ^a, P.C. Almond ^b, M.W. Hughes ^b

^a Department of Geological Sciences, University of Oregon, Eugene, OR, 97403, United States

^b Department of Soil and Physical Sciences, Lincoln University 7647, Canterbury, New Zealand

ARTICLE INFO

Article history:

Received 20 December 2008

Received in revised form 29 July 2009

Accepted 4 August 2009

Keywords:

Hillslope

Soil

Sediment transport

Mixing

Bioturbation

Tephra

ABSTRACT

In soil-mantled landscapes, downslope sediment transport occurs via disturbance-driven processes that vary with climate and vegetation change. To help constrain the long-term ($\gg 10$ yr) pattern and rate of soil mixing and transport in forests, we analyzed the distribution of tephra grains in soil along a hillslope transect in the Blue Mountains, SE Washington. Deposited within a loess mantle, tephra associated with Mt. Mazama (7.7 cal. kyr B.P.) serves as a marker bed for estimating erosion and transport rates. Moving downslope, the buried tephra horizon is progressively exhumed and becomes increasingly mixed in the upper soil layer, reflecting disturbance and transport via tree root growth and turnover. This pattern also implies increasing erosion rates downslope and our hillslope transect becomes increasingly convex coincident with progressive exhumation of the tephra layer. This systematic correspondence between topographic form, specifically, local convexity, and surface lowering is consistent with theoretical models for which soil transport rates depend on slope inclination. From our analysis, calibrated coefficients for a linear, slope-dependent transport model are on the order of $10^{-3} \text{ m}^2 \text{ yr}^{-1}$, consistent with previous work in forested loess-mantled landscapes. In addition, our results reveal both the high degree of soil mixing over millennial timescales and the local variability of mixing in forested landscapes. Furthermore, the results enable us to quantify the amount of energy expended by trees in mixing and transporting soil and the net sediment transport fraction of the net primary productivity NPP of the ecosystem.

Published by Elsevier B.V.

1. Introduction

During the Quaternary, climate change occurs over thousand-year timescales and many soil-mantled hillslopes have thus fluctuated between grassy and forested vegetative regimes. The morphologic legacy of different ecosystems, however, has not been addressed in the literature. Biotic processes are thought to play a major role in the evolution of hillslopes (Gilbert, 1909; Roering et al., 1999; Dietrich & Perron, 2006), but few studies have succeeded in quantifying the biotic role in sediment transport (Yoo et al., 2005). If vegetation influences transport processes, which in turn control landscape evolution, then the form of landscapes responds to and reflects climatic variation.

The transport of soil in the absence of overland flow has been attributed to processes such as soil creep, rain splash, variations in soil moisture (wet/dry) and temperature (freeze/thaw), tree throw (Lutz, 1960; Mort, 2003), and faunal burrowing/biogenic activity (Lutz and Griswold, 1939; Tyler et al., 2001; Yoo et al., 2005). The depth to which these processes occur, the soil above which is termed the active soil

layer or biomantle (Johnson, 1990), limits disturbance and transport of material by these agents. This layer can be less than the total soil depth, thereby forming an inactive soil layer, whose depth is equal to the distance between the bedrock and the active soil layer (Yoo and Mudd, 2008). The penetration of disturbances sets the thickness of the active soil layer (Heimsath et al., 2005) and, therefore, in thicker soils, net sediment fluxes (Roering, 2008).

In forests, root growth and tree uprooting has been shown to influence soil movement to such an extent that the ground surface is transformed into pit and mound topography (Denny and Goodlett, 1968) and soil profiles can become completely inverted or mixed (Schaezel, 1986; Small et al., 1990; Schaezel et al., 1990). In grassland soils populated by burrowing mammals, pedogenic evidence of mixing is also observed (Paton et al., 1995; Gabet et al., 2004; Yoo et al., 2005). In low-gradient terrain, disturbances on hillslopes promote soil transport at a rate directly proportional to hillslope gradient (McKean et al., 1993; Small et al., 1999). Biota, therefore, may be the major agent responsible for creating convex hillslopes, which are recognized as resulting from slope-dependent soil transport processes (Davis, 1892; Gilbert, 1909).

While most studies of soil mixing are relevant to short timescales (Walling and He, 1999; Tyler et al., 2001; Kaste et al., 2007), several recent papers have described soil mixing associated with geomorphic

* Corresponding author. Tel.: +1 541 346 4564; fax +1 541 346 2067.

E-mail address: swalther@uoregon.edu (S.C. Walther).

¹ Present address: Department of Geography, University of Oregon, Eugene, OR 97403, United States.

timescales. Evidence for soil mixing and transport due to tree turnover and root growth was documented in soil-mantled hillslopes on the South Island of New Zealand (Roering et al., 2002). During the forested Holocene, soil transport and erosion increased and exhumed and mobilized a tephra layer into the active soil layer where it became well mixed within the rooting zone. Also, vertical mixing rates have been documented in southeastern Australia using single-grain optically stimulated luminescence dating (Heimsath et al., 2002). Heimsath et al. (2002) showed that mixing depths and the degree of homogenization of tracer profiles vary through time owing to different climates. Long-term downslope movement and mixing of sediments has been successfully field-tested using ^{10}Be (McKean et al., 1993), short-lived fallout radionuclides (Kaste et al., 2007), and charcoal (Carcaillet, 2001) and tephra as a tracer (Roering et al., 2002, 2004a,b), although few studies have identified the transport mechanisms.

In this study, we quantify soil transport rates and document evidence of likely transport mechanisms in a forested ecosystem in the Blue Mountains of eastern Washington State. Our analysis, while similar to Roering et al. (2002), emphasizes local variability in mixing rates. For this analysis, we use tephra associated with the eruption of Mount Mazama (7720 cal. yr B.P.) to track soil mixing and erosion. The pit and mound topography that results from bioturbation (Schaezel et al., 1990; Gabet, 2000; Stokes, 2002; Gabet et al., 2003) is a reflection of stochastic soil transport processes. The goal of this study is to better understand the biological contribution to mixing and soil transport in forested landscapes. The main components of the study include using topography and the distribution of tephra to test and calibrate a soil transport model for a forested ecosystem. The use of tephra relies on the assumption that the glass grains are well preserved and geochemically immobile and therefore effective as particle tracers. Unlike fallout radionuclides, which only apply to the physical mixing at decadal scales, well-preserved tephra can be used to characterize physical mixing at millennial timescales. While cosmogenic radionuclides have also been applied for quantifying millennial scale soil mixing (Schaller et al., 2009), they cannot be applied universally and are time consuming and expensive. Our results are important for interpreting how vegetation affects rates of sediment production and the evolution of topography over geomorphic timescales.

2. Modeling soil transport

Convex slopes are found in many different climates and ecosystems. Owing primarily to disturbances (e.g. rain splash, tree throw, biogenic activity, soil creep, etc.), convex slopes are generally thought to result from slope-dependent transport in the absence of overland flow. Hillslope evolution has been numerically simulated using a conservation of mass equation and a slope-dependent transport model (e.g., Kirkby, 1971; Tucker and Bras, 1998). The linear, slope-dependent model that will be used as the basis for soil transport in this study is supported by field evidence (McKean et al., 1993; Gabet, 2000; Gabet et al., 2003) and is appropriate for gentle slopes (<60%). We use this model rather than a depth-dependent model (Heimsath et al., 2005) that varies as the product of slope and depth, because the depth of bioturbation appears to be relatively constant at our study site. In the two-dimensional version of the linear model, sediment flux, q_s ($\text{m}^3 \text{m}^{-1} \text{yr}^{-1}$), is linearly dependent on gradient according to:

$$q_s = K \nabla z \quad (1)$$

where K is the transport rate constant ($\text{m}^2 \text{yr}^{-1}$) and ∇z is the local topographic gradient (m/m). To calculate the evolution of the landscape surface due to soil transport, we combine Eq. (1) with a mass conservation equation to obtain an expression for erosion rate, E ($\text{m} \text{yr}^{-1}$), giving:

$$E = -K \nabla^2 z \quad (2)$$

This simplified formulation only addresses changes in the land surface due to erosion and does not consider contributions from rock uplift or variations in soil depth. In our study area, because more than 3 m of easily detachable material (loess) has accumulated over bedrock, the hillslope is effectively transport limited, so that its form is determined by transport processes, and Eq. (2) is appropriate. At the scale of the hillslope studied we can also neglect potential differences in rock uplift as an influence on hillslope morphology.

Eq. (2) can be applied to multiple locations along a slope to estimate differential erosion between the sites (Roering et al., 2002). The difference in erosion rates for two sites along a hillslope is given by:

$$E_A - E_B = -K(\nabla^2 z_A - \nabla^2 z_B) \quad (3)$$

where the A and B subscripts refer to erosion rate and curvature values for the two locations. If a stratigraphic layer was present in the hillslope soils at a consistent depth, and erosion has ensued for a known interval of time then erosion rates can be calculated using topographic data and Eq. (3) can be used to derive K . If the linear transport model is appropriate, a plot of differential erosion against differential curvature should exhibit a linear relationship with slope equal to K .

The transport coefficient K is an important parameter because it quantifies the efficiency of soil transport relative to hillslope gradient (Eq. (1)). Furthermore, it allows spatial variability of erosion rate to be calculated so long as hillslope curvatures are available from topographic surveys (Eq. (2)). This single parameter, however, encapsulates processes and factors which will vary between different landscapes. If biota are the dominant agent of soil disturbance and transport, then K essentially quantifies the energy expenditure of biotic processes in hillslope soils for a given ecosystem type. Yoo et al. (2005) adopted this conceptual framework to develop a model that related soil thickness, erosion rate and energy expended by gophers in the grass-covered coastal hills of California. Their model successfully predicted variation of soil depth on hillslopes according to gopher burrowing density. More studies are needed, covering a range of ecosystems, that relate K to biotic processes and thereby provide a process-based understanding of soil disturbance and transport on hillslopes (Roering, 2008).

3. Study site

Our study area is located in the northwestern Blue Mountains, Washington, a series of parallel mountains trending southwest-northeast that form the southern edge of the channeled scabland-Lake Missoula system. The study area is in the northwestern Blue Mountains on the margin of the channeled scablands and is underlain by Miocene Columbia River basalt characterized by horizontal and sub horizontal basalt flows. On the margin of the mountains, long ridges with flat interfluvial mirroring surfaces on basalt flows are separated by alluviated valleys with a total relief of about 1500 m. At our Robinette Mountain study site, hillslopes are the dominant landform as the mountains become higher and more finely dissected, ridges narrow and valleys become v-shaped and bedrock floored (Fig. 1).

The location of the study area near the scablands ensures that it has received significant loess deposition that blankets much of the Columbia Plateau. The characteristics of the Palouse loess that make it useful for paleopedologic and paleoclimatic research include its relative abundance, the presence of tephra layers that provide chronostratigraphic markers, and climatic, vegetative, and ecologic soil properties (Busacca et al., 2002). It is an ideal area to investigate the effect on sediment transport processes using tephra grains as tracers and here, we use the Mazama ash as a tracer to investigate hillslope transport processes. The Mazama tephra was deposited on top of loess and subsequently covered by loess. With time, the current

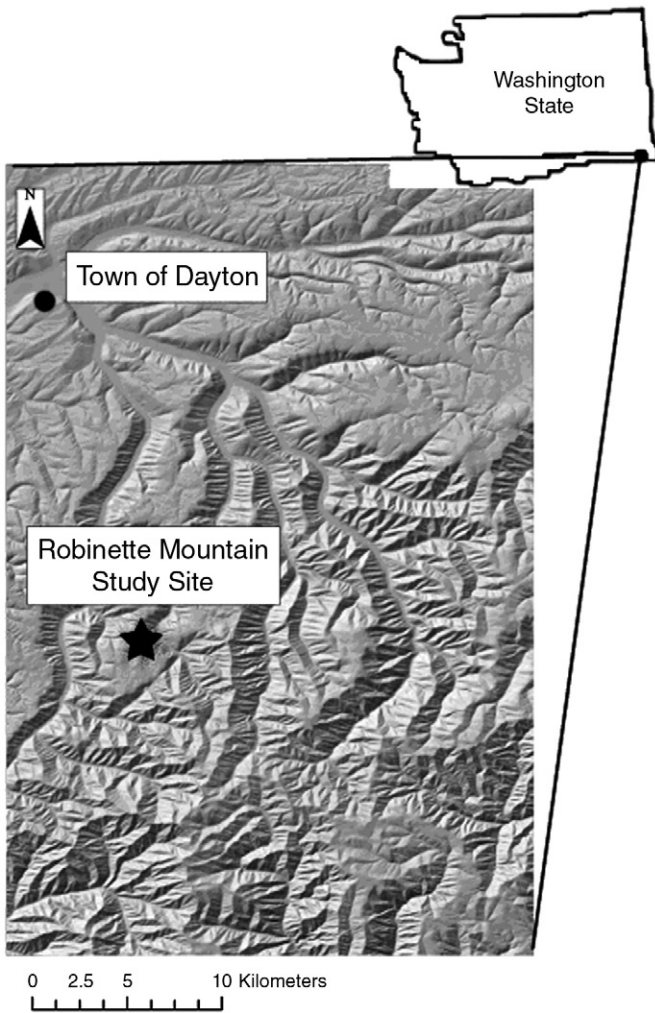


Fig. 1. Digital elevation model and hillshade of Robinette Mountain area with study site in the area of latitude 46.148°, longitude 117.9375°.

forests were established and bioturbation and erosion processes have exhumed the tephra layer (Fig. 2).

Four soil stratigraphic units from the late Quaternary have been named and several tephra layers have been correlated within the units (McDonald and Busacca, 1992; Busacca et al., 2002). Two major loess units of interest in this study span the last 70,000 yr and have been informally named L1 (the upper unit) and L2 (McDonald and Busacca, 1992). The most relevant tephra layer for this research is the Mazama tephra, found within the L1 loess unit. Mazama tephra has a ^{14}C age of 6845 ± 50 yr B.P. (Bacon, 1983) and a calibrated age of 7720 ± 55 yr ($1 - \sigma$). The radiocarbon date was calibrated with OxCal v3.10 (Bronk Ramsey, 1995; Bronk Ramsey, 2001) using the IntCal04 calibration curve (Reimer et al., 2004). This tephra layer is prevalent at shallow depths (<1 m) throughout the study area.

In the Columbia Basin, regional changes in vegetation are ascribed to large-scale changes in climate caused by spatial variations in the location of the Laurentide ice sheet and the varying length of the seasonal cycle of insolation (Blinnikov et al., 2002). The vegetation of the Plateau before modern agriculture ranged from sagebrush-steppe in zones of little precipitation, to meadow steppe in intermediate precipitation zones, to coniferous forest in wetter zones (Daubenmire, 1970). The early Holocene (11–7 kyr B.P.) was warm and dry due to high summer insolation (Blinnikov et al., 2002). Then, approximately 6 kyr B.P., forests expanded and moved to lower elevations, and the Blue Mountains have been continuously forested above 600 m ever since (Franklin and Dyrness, 1988). This reconstruction of the changes in the climate and vegetation, and the timing of forestation by Blinnikov et al. (2002) and Sweeney et al. (2006), enables us to use this site to study the influence of forest conditions on the hillslope transport processes.

The Blue Mountains today have a temperate dry climate caused by the Cascade rain shadow effect, with most precipitation occurring in winter (>1000 mm mean annual precipitation for the entire Blue Mountains) (Franklin and Dyrness, 1988). Three forest zones are found in the northern Blues Mountains at different elevations: *Abies lasiocarpa*–*Picea engelmannii* (>1500 m), *Pseudotsuga menziesii*–*Abies grandis* (900–1500 m), and *Pinus ponderosa* (600–1200 m) (Franklin and Dyrness, 1988). Our study site at Robinette Mountain is at 1200 m elevation, falling within the *Pseudotsuga menziesii*–*Abies grandis* and

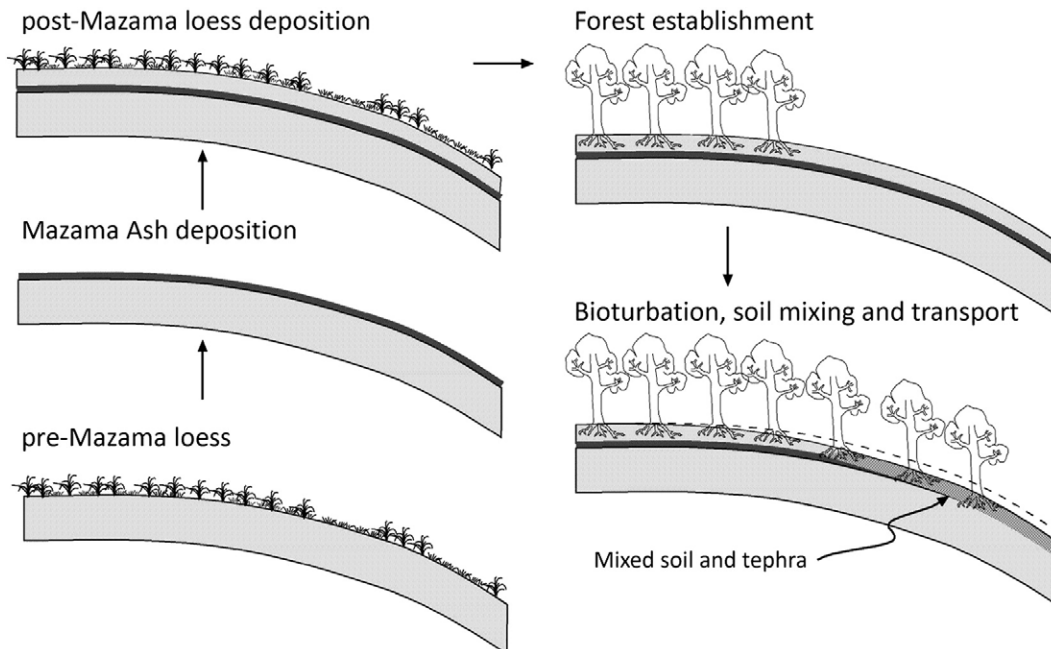


Fig. 2. Schematic of the landscape change from bottom left up and over to bottom right of pre-Mazama loess, deposition of Mazama tephra, subsequent loess deposition, establishment of the present-day forest, and finally, exhumation of the Mazama tephra via bioturbation and erosion.

Pinus ponderosa zones. It was chosen because of its location on conservation land so that shallow soils at the site would not be impacted by agriculture or ranching. The location of our study transect on the flanks of the Palouse hills has resulted in the deposition of enough loess to provide an excellent record and enough precipitation such that forest cover has been continuous since its establishment following rapid loess accumulation in the early to mid-Holocene (Sweeney, 2004).

4. Soil, tephra, and topography

4.1. Methods

In this study, we analyze soil properties and tephra distribution along a hillslope as a reflection of transport rates and mechanisms. Two pits and four sets of auger holes were excavated at points along a hillslope transect (Fig. 3). We sampled depth variations in tephra concentration and soil properties from the auger holes and soil pits. To obtain meter-scale hillslope morphology (and estimates of local curvature as required by Eq. (2)), hundreds of topographic data points were obtained using a Total Station.

Our sampling sites were located along a convex hillslope. We collected soil samples from four sites on the hillslope at 5 cm and 10 cm intervals for the two pits and the four sets of augered cores, respectively. Using a hand-hammer-corer fashioned from a 5.7 cm diameter metal pipe, we took the samples from the sidewalls within each pit in 5 cm increments. For the three auger sites, we took four cores at 10 cm intervals and combined them at each interval to average the sample at that depth and reduce the effect of rooting, burrowing, and infilling from tree root mixing and bioturbation (documented in the loess at lower elevations) (O'Green and Busacca, 2001). Similarly, from the two pits, we took three samples at 5 cm intervals and combined them at each interval. Soils were classified according to horizon (Birkeland, 1999) and described using Munsell colors (Munsell, 1976) in Appendix A of Walther (2006).

In order to determine the gradient and the curvature of the slope, we used the topographic data from local patches of survey data around each of the soil pit and auger sites. In doing so, we used the topographic data points within 6 different radii (2-, 5-, 7.5-, 10-, 12-, and 15-m) to determine the most appropriate scale of topographic derivatives for calculating the curvature of the sites. From the

topographic data (x , y , and elevation z data points), we fit a second-order polynomial and used the coefficients of the variables to determine the gradient and the curvature of the local hillslope (Appendix C, Walther, 2006).

After calculating the dry soil density, we ground the aggregates using a mortar and pestle, sieved the soil, and kept the <2 mm fraction. Next, we treated 20 g of subsamples with hydrogen peroxide to remove organic matter. Then, we used a citrate–dithionite–bicarbonate reagent and adapted from the method of Blakemore et al. (1987) to remove oxide coatings. Then, we washed, sieved to isolate the 63–200 μm grain-size fraction, filtered, dried at 60 °C, and weighed the samples (Appendix D, Walther, 2006). This size fraction contains the majority of tephra grains at this locale.

To count the glass grains in the samples, we employed a spiking technique used extensively by P. Almond at Lincoln University, New Zealand, similar to those used in pollen analysis (Faegri et al., 1989; Whitlock et al., 2000; Brunelle et al., 2005). With this technique, a subsample of the 63–200 μm fraction was spiked with a precisely determined mass of Ballotini™ silica abrasion beads that amounted to 20% of the original sample weight. Using the manufacturer's specifications of number of grains per gram of beads we calculated the number of spike grains per gram of sample-plus-spike mix. After shaking for 15 s, grains of this mix were placed in the well of a microscope slide and then mixed in three drops of clove oil mounting medium. We then placed the slide under a microscope (Leica 10 \times –40 μm) where grains of volcanic glass and spike grains were counted as follows. A location on the slide was selected and all visible spike and glass grains were counted. These data were plotted on a graph of glass grains versus spike grains and then a new location was selected. The counts of glass and spike grains at the new location were then added to the counts from the previous location and plotted. This procedure continued, plotting cumulative glass grain count versus cumulative spike grain count, until the plot formed a relatively straight line. The slope of this line represents the ratio of glass grains to spike grains. In most samples a straight line resulted after we counted about 5 or 6 locations. Given the known concentration of spike grains, the ratio of glass grains to spike grains was used to calculate the concentration of glass grains per g of 63–200 μm material.

4.2. Results

4.2.1. Soil morphology and stratigraphy

Soils in the area are mapped as Tolo silt loam (Andic Vitrixerand) (Soil Survey Staff, Natural Resources Conservation Service, United States Department of Agriculture Web Soil Survey (Available online at <http://websoilsurvey.nrcs.usda.gov/> accessed [10/14/2008]) in recognition of the dominance of andic soil materials derived from Mazama ash in the upper part of the soil. Pit A on the hilltop at our study site revealed 2 cm of forest litter over a thin (0–3 cm) A horizon above a 50 cm thick high chroma (10YR 5/6) silt loam Bw horizon with low bulk density and crumb structure. This material overlies the buried Washtucna soil, which at our site comprised two horizons; the uppermost, a 9 cm thick, pale (10 YR 6/1), buried E horizon (top at 53 cm depth) with moderately firm soil strength and a brittle failure. The lower horizon was a 60 cm thick, hard, brittle and dense, fragipan (Bxg) with silt loam texture. The fragipan had a mottled color pattern of 2.5 YR 5/3 and 10 YR 6/1. Below 120 cm our description was made by hand augering, and it revealed two additional buried E horizon/Bx horizon couplets of silt loam texture. Bedrock was reached at 2.30 m depth.

Pit C, 22 m from the hilltop, showed a similar stratigraphy but the surface soil was thinner and showed considerable profile variability around the pit with some redoximorphic features. On the SW pit wall, andic soil material, comprising an A and Bw horizon, extended to only 15 cm depth. This was underlain by a pale, blocky structured Bg horizon with pods of Mazama ash between 25 and 30 cm depth. On

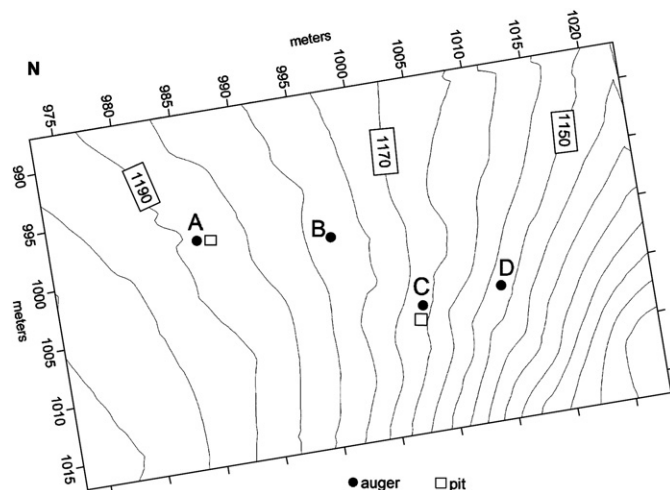


Fig. 3. Digital elevation model (or topographic map) of sampling sites on the hillslope. Actual elevations are inserted into the figure, while the scale on the map is local (relative) coordinates. Site A includes pit and auger sampling. Site B, 11 m downslope from A, includes auger sampling. Site C, 20 m downslope from A, includes another pit (2 sets of samples) and auger sampling. Site D, 26 m downslope from A, samples were from augering.

the NE wall (Fig. 4), a similar profile form was broken by a pocket of orange-colored andic material extending to 60 cm depth. This material was crudely stratified, alternating in texture between silt loam and sandy loam, and was of high chroma, varying between 10YR 4/4, 5YR 5/8 and 7.5YR 4/6 with increasing depth. Both pit faces were sampled, and glass counts supported our field interpretation (Fig. 5), showing low glass grain counts, concentrated in the upper 15 cm, in the SW wall, and much higher glass grain counts throughout the upper 45 cm of the NE wall andic material pocket, with the greatest concentration in the bright orange (7.5YR 4/6) material at the base. A concentration of charcoal occurred between 45 and 50 cm depth.

Beneath the surface soil, at 45–60 cm depth, was a pale, dense, blocky to prismatic-structured, silt loam, buried E horizon that graded downwards into a mottled fragipan (Bxg), corresponding to the Washtucna soil. Augering below 90 cm depth suggested another E/Bx couplet between 90 cm and 170 cm, below which bedrock was met.

4.2.2. Tephra distribution

In order to characterize the pattern of exhumed and transported tephra along our transect, we estimated the total glass inventory and the average concentration for each sampling site to a depth of 80 cm (Table 1). This allows for comparison of the distribution with depth and the average concentration at each interval between the sites. We expect that biomantle thickness does not vary significantly between our sites such that average concentrations will reflect variations in landscape lowering. At depths greater than 80 cm, the glass counts diminish to nearly zero and are therefore considered negligible. The individual grains do not exhibit visible alteration (Appendix B, Walther, 2006), supporting the use of the tephra grains as a conservative tracer at this site.

The shapes of the distribution profiles at each of the sites are similar in that they are relatively asymmetric around the concentration peak. The distributions are positively skewed, with a thicker tail above the peak and a thinner and narrowing tail below the peak.

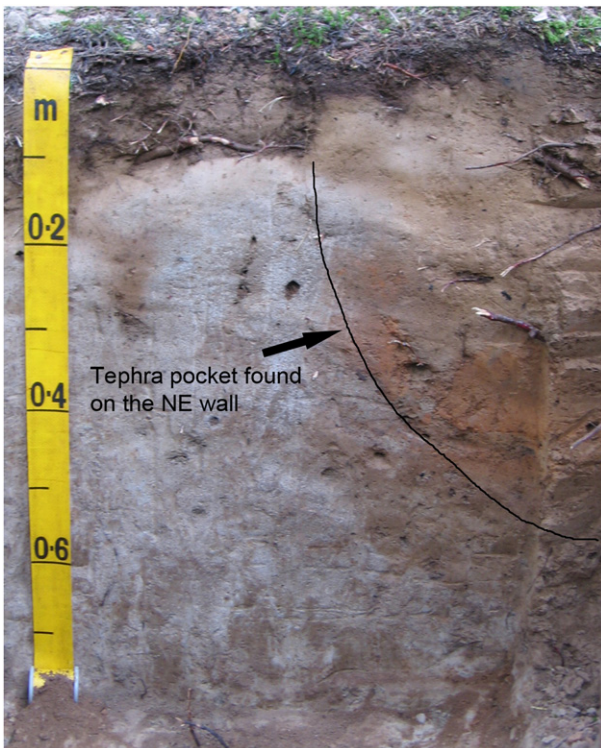


Fig. 4. Photo of site C. Note the pocket of tephra on the NE Wall. This pocket lead us to sample the pit in two corners, as well as augering the site, thereby giving us three sets of tephra values for site C as graphed in Fig. 5.

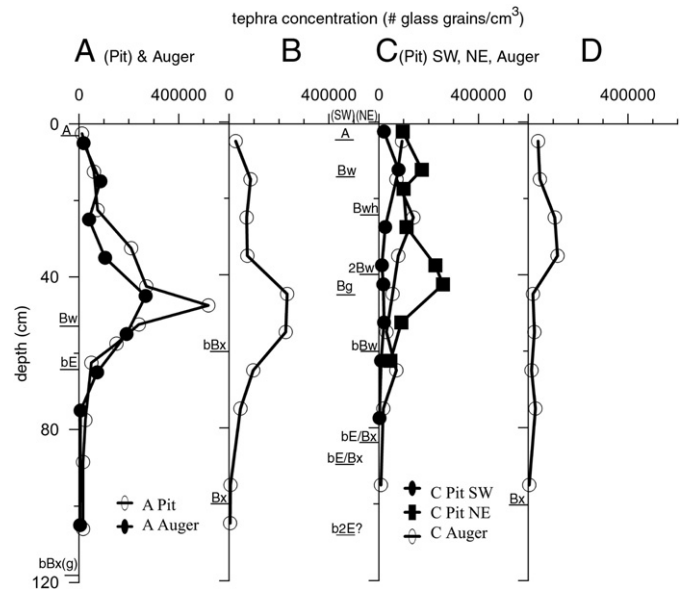


Fig. 5. Tephra concentration depth profiles for each site. Concentrations are inventories in 10 cm depth increments and are expressed as grains/cm³ (grains/cm² divided by depth interval (cm)). Soil horizons are included on the left side of the y-axis of the corresponding tephra profile.

Overall, the depth to peak concentration becomes shallower downslope (Fig. 5).

Moving downslope, the distribution at site A has a peak at 45–50 cm with a thicker, irregular tail above the peak (shallower) and a thin, narrowing tail below the peak (deeper). The tephra peak occurs within a thin, centimeter-scale layer of slightly lighter, whitish to pale orange soil at a depth of 45–50 cm. The soil stratigraphy at our study site may reflect an important process linkage with the distribution of roots and biomass that may drive soil mixing and transport. Root distributions, for both globally averaged data and forested ecosystem specific data, universally show a rapid decay of density with depth (Schulze et al., 1996; Jackson et al., 1996). Because of variability in bioturbation and rooting depths, some tephra remained at A, the topmost site. The tephra peak is located in the Bw horizon, a silt loam with a low bulk density, and a weak, fine blocky and crumb structure. The soil becomes firmer between 43 and 53 cm, approximately where the tephra peak is located. This firmer, brittle consistency is also characteristic of the tephra found in the C-NE site described below.

The shape of the site A auger-generated tephra distribution is similar to that of the site A pit-derived tephra distribution, but the height of the peak is smaller and the mixing above the tephra peak appears more uniform. This, in part, reflects the different sampling intervals between the two, with pit A sampled at 5 cm intervals and the auger sampled at 10 cm intervals. We use the peak position located from the pit sampling for the erosion rate calculations because of the higher resolution of the sampling. Site A has the highest glass

Table 1

Total glass inventories and average tephra concentrations for each site.

| Pit/auger site | Gradient | Curvature | Total glass inventory (# glass grains/cm ²) | Average concentration (# glass grains/cm ³) |
|----------------|-----------------------|------------------------|---|---|
| A (Pit) | 9.09×10^{-2} | -5.06×10^{-3} | 1.08×10^7 | 1.35×10^5 |
| A (Auger) | 9.09×10^{-2} | -5.06×10^{-3} | 7.94×10^6 | 9.92×10^4 |
| B (Auger) | 1.21×10^{-1} | -6.74×10^{-3} | 8.81×10^6 | 1.10×10^5 |
| C-NE (Pit) | 2.11×10^{-1} | -1.21×10^{-2} | 8.78×10^6 | 1.35×10^5 |
| C (Auger) | 2.11×10^{-1} | -1.21×10^{-2} | 5.67×10^6 | 7.09×10^4 |
| C-SW (Pit) | 2.11×10^{-1} | -1.21×10^{-2} | 2.06×10^6 | 2.58×10^4 |
| D (Auger) | 2.53×10^{-1} | -1.10×10^{-2} | 4.10×10^6 | 5.13×10^4 |

inventory (largest number of grains/cm²) and average concentration (largest number of grains/cm³), with the exception of site C-SW described below.

The site B tephra concentration distribution exhibits a broad peak between 40 and 60 cm, with two samples in that zone that are indistinguishable. The general shape of the distribution of tephra at site B is similar to that of site A, with approximately the same depths of the peaks. However, the peak in the B distribution is much more subdued: the peak is smaller and mixing above the peak appears more uniform.

Because of variable nature of soil characteristics observed in the pit at site C, we sampled from the NE corner (assumed tephra pocket) and the SW corner of the pit, as well as nearby auger holes. The tephra concentration profiles at site C exhibited a wide range of concentrations and differences in concentration peak depths. The shape of the distribution of tephra at C-SW includes a small and shallow peak at approximately 15 cm, with a diminished tail below the peak. The shape of the distribution of tephra at C-NE, is different in that it includes a peak just below 40 cm depth, with variable mixing of tephra above the peak and decreasing concentrations below the peak (sampling stopped at 65 cm). The concentration of charcoal found at a depth of 45–50 cm corresponds with the largest concentration peak at just over 40 cm. The shape of the distribution for the C-Auger samples includes a tephra peak at approximately 25 cm, with uniform mixing above the peak and a rapid drop in tephra concentration below the peak. The tephra concentration peak in the C-Auger profile appears to be almost intermediate between the C pit (NE and SW) concentration peaks in both depth and in concentration. The tephra inventory is lowest at C-SW (2.06×10^6 grains/cm²) and highest at C-NE (8.78×10^6 grains/cm²), with the C-Auger counts falling between the other two (5.67×10^6 grains/cm²), only slightly more than the average of the two sampling areas in the pit (5.42×10^6 grains/cm²).

The tephra concentration profile at site D shows a broad peak that is located over two sampling points (augered) between 20 and 40 cm. There is very little tephra above the peak and even less immediately below it. The tephra inventory (4.10×10^6 grains/cm²) is lower than the other sites (with the exception of C-SW).

4.2.3. Hillslope morphology

We quantified the morphology of the study transect to relate changes in tephra depth and extent of mixing to transport rates for this forested ecosystem. Given that local topography in the forest is relatively hummocky (as generated via tree turnover), we sought to estimate curvature values representative of the coarser hillslope rather than the localized topographic anomalies associated with individual trees (Heimsath et al., 1999). As such, we varied the radius used to obtain the local patch of points between 2 and 15 m (Fig. 6).

Curvature values for our sites are extremely variable at the 2 m and 5 m radius ranges (Fig. 6), reflecting the pit and mound topography of the forest floor. The curvature determined from the 7 m radius exhibits some variability, but not as much as with the smaller radii. For radii greater than 10 m, the curvature values become roughly consistent and the number of input data points is sufficiently large enough to obtain a representative curvature of the hillslope at that site. The r^2 values for the polynomial fits also increased with radius and for radii greater than 10 m, the r^2 values became constant at ~ 0.90 . Based on this analysis, we selected a 10 m radius to calculate curvature values for our soil sampling sites. In support of this choice, the 10 m radius is greater than the scale of pit and mound topography observed (roughly around 2–3 m) at our study site.

Using a 10 m radius, we estimated hillslope gradient and curvature at our soil sampling sites. Site A, near the crest of the hillslope and at the top of the transect, has low values of gradient and curvature (Table 1). The gradient increases with distance downslope from the crest, with the steepest value at site D. This increase in gradient

downslope defines a convex form. According to Eq. (1), sediment flux should be greatest at site D and decrease upslope.

5. Transport model calibration

5.1. Methods

The tephra concentration peak provides a datum from which to quantify the amount of erosion at a site: at sites with more erosion the tephra concentration peak is shallower, and at sites less affected by erosion it is deeper. Specifically, we compare the depths of tephra peak concentration between the hilltop (Site A) and individual sites on the hillslope to calculate differential erosion (Eq. (3)). The assumptions involved in this approach include: 1) the peak is still observable (although it may be attenuated in areas of rapid lowering) and 2) the decrease in depth to the peak is a result of erosion. To calculate differential erosion rates, we use the time elapsed since deposition of Mazama ash (7720 cal. yr B.P.). Between 7720 cal. yr B.P. and 6000 cal. yr B.P. loess was still accumulating on a grass/shrubland covered landscape after which forest recolonized (Sweeney et al., 2006). This results in a small error in calculating a K value appropriate to a forest ecosystem as discussed below.

5.2. Results

By comparing the depth of the tephra peak at site A with peak depths at sites B through D, we calculated differential erosion rates ranging from 0.003 to 0.045 mm yr⁻¹ (Table 2). For each combination, we also calculated differential curvature. Differential erosion rate varies linearly with differential curvature ($r^2 = 0.77$, $p < 0.01$; Fig. 6). The slope of the line defines the transport coefficient, K , to be 0.0048 ± 0.0007 m² y⁻¹.

The mechanical power of soil transport processes can be calculated using a relationship first proposed by Roering et al. (1999) as:

$$K = [P / (\rho_s g \mu^2)] \quad (4)$$

where P is the power input per unit area (MT⁻³), ρ_s is the soil bulk density (ML⁻³), g is the gravitational acceleration constant (LT⁻²), and μ is the effective coefficient of friction. Yoo et al. (2005)

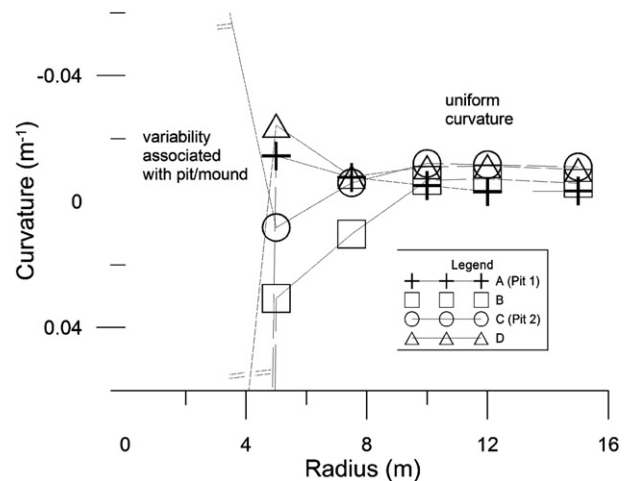


Fig. 6. Curvature determined from topographic data points within a radius ranging between 2 m and 15 m. This was done to select a radius of data points for the given landscape from which to determine a representative curvature. Note that the curvatures for the sites are extremely variable at the 2 m and 5 m radii, reflecting the pit and mound topography of the forest. The curvature from the 7 m radius data exhibits less variability, as the curvatures begin to smooth out with a greater radius and therefore a greater number of input data points. For radii of 10 m and greater, the curvature becomes more uniform and the number of data points is large enough to obtain a curvature of the hillslope instead of small-scale deviations in topography.

Table 2

Erosion rate and curvature differences between sites on the hillslope and the hilltop, starting with the difference between site A and B (shown at B), and so on going downslope.

| Pit/auger Site | Differential erosion rate $\Delta z / \Delta t$ ($10^{-6} \text{ m yr}^{-1}$) | Differential curvature $\Delta (\partial^2 z / \partial x^2)$ (10^{-3} m^{-1}) |
|----------------|---|--|
| B | 3.2 ± 2 | 1.7 ± 0.2 |
| C | 29 ± 2 | 7.1 ± 0.2 |
| D | 23 ± 3 | 6.0 ± 0.2 |
| C-SW | 45 ± 2 | 7.1 ± 0.2 |

partitioned the power term to solve for the power input of dominant biota in a given ecosystem:

$$K = [NP_i / (\rho_s g \mu^2)] \quad (5)$$

where N is the population density of the organism (L^{-2}) and P_i is the individual power input (ML^2T^{-3}). From our estimated transport coefficient values ($4.8 \times 10^{-3} \pm .0007 \text{ m}^2 \text{ y}^{-1}$), the average soil density of the study site samples (1.07 g cm^{-3}), and the effective coefficient of friction (1.27 from Roering et al., 1999), we first estimated the power input per area (NP_i) for the forest and then calculated power for individual trees in the stand (Table 3). The estimated power of the ecosystem is $83 \text{ J m}^{-2} \text{ yr}^{-1}$. Using a tree stand density of 249 ha^{-1} ($2.5 \times 10^{-2} \text{ m}^{-2}$) for a mature mixed conifer forest (diameter 5 cm and greater) in eastern Washington (Lehmkuhl et al., 2006), we estimated the power of an individual tree to be $\sim 3.3 \text{ kJ yr}^{-1}$. The power of the forest ecosystem ($83 \text{ J m}^{-2} \text{ yr}^{-1}$) is somewhat less than that estimated by Yoo et al. (2005) for a coastal California grassland ($\sim 80\text{--}120 \text{ J m}^{-2} \text{ yr}^{-1}$). Yoo et al. (2005) estimated the power input of the dominant biota, pocket gophers, which have a slightly lower density ($\sim 140 \text{ ha}^{-1}$) than trees at our study site. In terms of ecosystem energy, the net sediment transport at their site is $\sim 0.001\%$ of the net primary productivity (NPP) in California grasslands, when using a value of $\sim 3.3 \text{ MJ m}^{-2} \text{ yr}^{-1}$ (Callaway et al., 1991). For our forested ecosystem, the fraction of net sediment transport is 0.002% of the Blue Mountain NPP of $5.3 \text{ MJ m}^{-2} \text{ yr}^{-1}$ (Hudiberg et al., 2009). These fractions are close in value because the transport rates are similar and the NPP values are not that different. The grassland and forest ecosystems have similar results, suggesting that geomorphic work may be a small fraction regardless of the ecosystem.

6. Discussion

6.1. Tephra distribution profiles

The positively skewed shape of the tephra profile distributions is evidence of upward mixing of tephra from a primary emplacement horizon. Some of this mixing may have occurred between 7720 yr B.P. and 6000 yr B.P. while loess was accumulating, but this phase is very unlikely to account for the decrease in total tephra inventory downslope, and hence other mixing processes are implicated. Tephra

Table 3

Power input per area of the system and of individual trees estimated from the mean transport coefficients of the marker method.

| Mean K ($\text{m}^2 \text{ yr}^{-1}$) | NP_i ($\text{J m}^{-2} \text{ yr}^{-1}$) | P_i (kJ yr^{-1}) |
|--|---|----------------------------------|
| 0.0048 | 81 | 3.3 |

The estimate of NP_i used a bulk soil density of 1.07 g cm^{-3} (this study), the gravitational acceleration constant of 9.8 m s^{-2} , and an effective coefficient of friction of 1.27 (Roering et al., 1999).

The estimate of the power input of the individual trees used a stand density (N) of $249 \text{ trees ha}^{-1}$ (Lehmkuhl et al., 2006).

grain concentrations are most uniformly distributed in the top 40 cm of the soils, which is consistent with the depth of bioturbation under forest, revealed by other tracer studies (Roering et al., 2002), and with the vertical distribution of roots documented for a similar forest. Roering et al. (2003) and Schmidt et al. (2001) report that 50% of the root network in western Oregon conifer forest occurs above 40 cm depth.

We propose that forest bioturbation is the major mixing mechanism and that it also drives downslope soil transport. The linear relationship between erosion rate and hillslope curvature (Fig. 7) indicates that the transport processes responsible for erosion show a linear dependence on hillslope gradient (Eqs. (1) and (2)). This kind of dependency usually arises where soil disturbance and gravitational settling dominate soil transport. At our site it appears that the agent of disturbance relates to trees, probably both in respect of the disturbances caused by soil dilation as tree roots grow (Schaezel et al., 1990; Stokes, 2002; Mort, 2003) and by tree throw (Gabet, 2000; Gabet et al., 2003).

The downslope decreases in tephra inventory and concentration reflect the progressive exhumation of the primary tephra layer with increasing erosion rate. As the ground surface lowers and the tephra enters the upper 40 cm thick, actively mixed layer the probability of it being disturbed by root growth and upheaval increases. The downslope direction favors increasing loess exhumation and transport of tephra grains, and the incorporation of tephra-poor loess from beneath the primary emplacement horizon causes a decrease in tephra concentration.

While the sampling strategy we employed (aggregating several samples from the same depth at a locale on the hillslope as well as sub-sampling a pit) has demonstrated systematic trends in soil erosion in relation to hillslope morphology, it has also identified the spatial heterogeneity of bioturbation processes. At site C the variability of the tephra depth profiles and total inventories in the opposite faces of the pit probably reflect localized differences in tree root density and dilation and of the frequency of turnover events. Norton (1989) proposed an exponential model to describe the rate of turnover of forest soil. According to the model, the probability that a new patch of soil is disturbed with each generation of forest decreases exponentially as the likelihood of trees reoccupying already-disturbed sites increases. Norton (1989) defined a turnover half-life dependent on average tree lifespan and forest density to characterize the temporal progress of soil turnover. Even after many millennia, local patches of soil can remain undisturbed. The similarities between the tephra peak depths and the inventories between site A and the NE wall of the pit at site C, and the very low inventory in the SW wall of the same pit, suggests that our excavation straddled sites of minimal and significant disturbance. We avoided obvious pit or mound

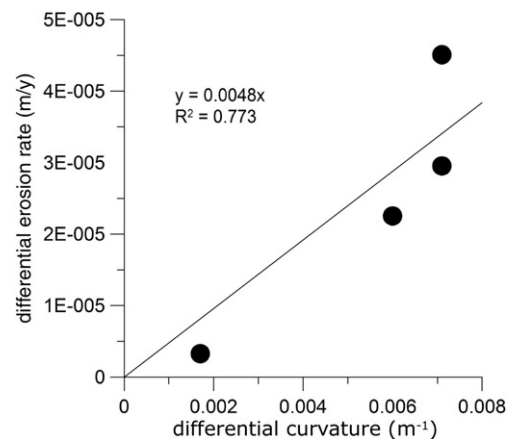


Fig. 7. Differential erosion rate of hillslope sites relative to site A (hilltop) plotted against differential curvature, again relative to site A. The significant linear relationship ($p < 0.01$) and high r^2 support the use of a linear slope-dependent transport model.

topography in our sampling but we may have sampled the boundary of a previous generation of topography that has since been diffused.

Our results provide a long-term perspective of bioturbation seldom addressed by other approaches (Roering et al., 2002; Schaller et al., 2009). Fallout nuclides, for example, sample decadal time periods and thus are unlikely to be representative of geomorphically-relevant forest dynamics. For a tracer layer (^{137}Cs) that was relatively recently deposited and is located near the top of the soil column, for example, a downward decrease in the tracer was attributed to bioturbation (Tyler et al., 2001). Conversely, in the same study, the absence of evidence for the mixing of tracers was used to indicate the lack of bioturbation. In our study, the tephra at all of the sampling sites shows evidence of mixing.

6.2. Estimating K

Because our approach uses the depth to the tephra peak for estimating K , it is relatively insensitive to variability in mixing that affects the magnitude of the tephra peak. Our K value ($0.0048 \pm 0.0007 \text{ m}^2 \text{ yr}^{-1}$) is similar in magnitude to other estimates in forested ecosystems (Nash, 1980; Reneau and Dietrich, 1991; Roering et al., 1999; Almond et al., 2008) and an order of magnitude greater than estimates obtained in arid environments (Colman and Watson, 1983; Hanks et al., 1984; Hanks, 2000). Our value is lower than those found on a deeply rooted forested ecosystem (Roering et al., 2002) and then on grassy, mudstone hillslopes (McKean et al., 1993). The transport coefficient estimates the activity of the processes contributing to sediment transport for a given landscape. In a forested ecosystem K represents processes such as tree turnover, root growth, faunal borrowing (gophers, worms, etc.).

6.3. Sources of uncertainty

Our estimate of K is an average over two potentially different soil transport regimes. The first corresponds to the approximately 1700 yr between the deposition of Mazama ash and 6000 cal. yr B.P. when the site was grassland/forest transition (or a parkland), and during which time loess was still accumulating. The second corresponds to the period since 6000 yr B.P. when the area was reforested, and loess deposition had ceased. Assuming a uniform loess accretion rate across the hillslope, any coeval soil transport would have resulted in a spatially variable accumulation rate and a non-uniform loess thickness along the slope. Any initial differences in loess thickness resulting from soil transport during loess accretion are subsumed within our erosion rate calculations and contribute uncertainty to our forest K value. The magnitude of the error depends on the relative erosion rates between the shrubland/grassland and the succeeding forest, and the duration over which the respective soil transport regimes operated. The 1700 yr of loess accumulation in a shrubland/grassland-covered slope amounts to 22% of the time since Mazama ash was deposited, and therefore soil transport under this regime was likely minor component of total post-Mazama transport. Observations at nearby sites suggest minor mixing of loess following Mazama ash deposition. Comparisons of soil transport rates under forest versus under grassland/shrubland (Roering et al., 2004a,b; Almond et al., 2008; Hughes et al., 2009) suggest rates under forest are greater, in which case our calculated K value is an underestimate. If no erosion occurred in the period 7720 yr BP to 6000 yr BP, a uniformly thick loess mantle would have covered the slope, all erosion would have taken place in the subsequent 6000 yr period, and our estimate of K , and power expenditure by the forest are ~20% too low.

Other uncertainties that arise in the tephra data result from differences in the sampling intervals between the pits and the auger-cores (5 cm and 10 cm, respectively). For example, at the B and D sites, the tephra concentration peaks are somewhat subdued and do not necessarily capture the peak magnitude. Additionally, our method assumes that the silica abrasion beads are homogeneously mixed.

Furthermore, based on previous work in the area (Busacca et al., 1992; Blinnikov et al., 2002), we assume that the tephra is composed only of Mazama ash. Mazama tephra is almost certainly the dominant source of tephra grains, and even if cryptotephra from other volcanic ashes were present it is very unlikely to influence our results since our analysis is based on depth to tephra peak concentration not total tephra grain inventory.

7. Conclusions

This study quantifies aspects of soil mixing and transport on a forested hillslope, including power expenditure and transport coefficient (K). On our low-gradient study transect, the relationship between erosion rate and hillslope curvature suggests soil transport rate varies linearly with hillslope gradient. The spatial distribution of tephra serves as a marker for soil transport in that the depth of the peak and the distribution of volcanic glass represents the exhumation of the tephra layer and provides evidence for the mixing and movement of soil by mechanisms such as root growth, bioturbation, and tree throw.

Topographic data obtained on our study hillslope were used to estimate curvature along the hillslope transect. To generate geomorphically-relevant curvature values, a minimum radius of 10 m is needed to average over noisy local hillslope topography due to tree-throw pits and mounds. Our method uses changes in the depth of the tephra peak downslope to calculate relative rates of landscape lowering due to soil transport. Our estimated value of K is 0.0048 ± 0.0007 , which is similar to values obtained in other forested ecosystems.

Our results constrain the post-Mazama deposition transport coefficient for a mountainous, forested landscape and can be used for modeling hillslope evolution and sediment transport in similar settings. Attributing the K values to the disturbance-driven processes associated with a forest, suggests that the K values may be different for grassland ecosystems as disturbance rates could be suppressed in grass-covered ecosystems. This approach enables us to evaluate the fraction of geomorphic power expenditure based on ecosystem. The fraction of net sediment transport in our forest ecosystem has similar results to that of the grassland of Yoo et al. (2005), suggesting that geomorphic work may be a small fraction regardless of the ecosystem.

Acknowledgments

This study was supported by National Science Foundation grant EAR-0309975. We thank the Confederated Tribes Umatilla Indian Reservation (CTUIR) for access, K. Yoo for thoughtful review of the manuscript, and T.C. Hales and R. Harrel for help in the field.

References

- Almond, P.C., Roering, J., Hughes, M., Lutter, F.S., LeBoutieller, C., 2008. Climatic and anthropogenic effects on soil transport rates and hillslope evolution. *Sediment Dynamics in Changing Environments*, Christchurch, New Zealand: IAHS, Publication, vol. 325, pp. 417–424.
- Bacon, C.R., 1983. Eruptive history of Mt. Mazama and Crater Lake caldera, Cascade Range, U.S.A. *Journal of Volcanology and Geothermal Research* 18, 57–115.
- Birkeland, P.W., 1999. *Soils and Geomorphology*, 3rd Edition. Oxford University Press, Oxford.
- Blakemore, L.C., Searle, P.L., Daly, B.K., 1987. Methods for chemical analysis of soils. NZ Soil Bureau Scientific Report 80, NZ Soil Bureau, Lower Hutt.
- Blinnikov, M., Busacca, A., Whitlock, C., 2002. Reconstruction of the late Pleistocene grassland of the Columbia basin, Washington, USA, based on phytolith records in loess. *Palaeogeography, Palaeoclimatology, Palaeoecology* 177, 77–101.
- Bronk Ramsey, C., 1995. Radiocarbon calibration and analysis of stratigraphy: the OxCal Program. *Radiocarbon* 37 (2), 425–430.
- Bronk Ramsey, C., 2001. Development of the Radiocarbon Program OxCal. *Radiocarbon* 43 (2A), 355–363.
- Brunelle, A., Whitlock, C., Bartlein, P., Kipfmüller, K., 2005. Holocene fire and vegetation along environmental gradients in the Northern Rocky Mountains. *Quaternary Science Reviews* 24 (20–21), 2281–2300.
- Busacca, A.J., Nelstead, K.T., McDonald, E.V., Purser, M.D., 1992. Correlation of distal tephra layers in loess in the channeled scabland and Palouse of Washington. *Quaternary Research* 37, 281–303.

- Busacca, A.J., Gaylord, D.R., Sweeney, M.R., 2002. Paired eolian deposits and megaflood features, Columbia Plateau, Washington. Friends of the Pleistocene 10th Annual Pacific Northwest Cell Field Trip Manual, p. 80.
- Callaway, R.M., Nadkarni, N.M., Mahall, B.E., 1991. Facilitation and interference of *Quercus douglasii* on understory productivity in central California. *Ecology* 72, 1484–1499.
- Carcaillet, C., 2001. Are Holocene wood–charcoal fragments stratified in alpine and subalpine soils? Evidence from the Alps based on AMS ^{14}C dates. *The Holocene* 11 (2), 231–242.
- Colman, S.M., Watson, K., 1983. Ages estimated from a diffusion equation model for scarp degradation. *Science* 221 (4607), 263–265.
- Daubenmire, R., 1970. Steppe vegetation of Washington. Washington Agricultural Experiment Station. In: Technical Bulletin, vol. 62. Washington State University, Pullman.
- Davis, W.M., 1892. The convex profile of bad-land divides. *Science* 20, 245.
- Denny, C.S., Goodlett, J.C., 1968. Tree-throw origin of patterned ground on beaches of the ancient Champlain Sea near Plattsburgh, New York. US Geological Survey Professional Paper, vol. 600-B, pp. B157–B164.
- Dietrich, W.E., Perron, T., 2006. The search for a topographic signature of life. *Nature* 438 (26), 411–418.
- Faegri, K., Kaland, P.E., Krzywinski, K., 1989. Textbook of Pollen Analysis. Wiley, New York, 328 pp.
- Franklin, J.F., Dyrness, C.T., 1988. Natural Vegetation of Oregon and Washington. Oregon State University Press, Corvallis, OR.
- Gabet, E.J., 2000. Gopher bioturbation: field evidence for non-linear hillslope diffusion. *Earth Surface Processes and Landforms* 25, 1419–1428.
- Gabet, E.J., Reichman, O.J., Seabloom, E.W., 2003. The effects of bioturbation on soil processes and sediment transport. *Annual Review of Earth and Planetary Sciences* 31, 249–273.
- Gabet, E.J., Pratt-Sitaula, B., Burbank, D.W., 2004. Climatic controls on hillslope angle and relief in the Himalayas. *Geology* 32 (7), 629–632.
- Gilbert, G.K., 1909. The convexity of hillslopes. *Journal of Geology* 17, 344–350.
- Hanks, T.C., 2000. The age of scarplike landforms from diffusion–equation analysis. In: Noller, J.S., et al. (Ed.), *Quaternary Geochronology: Methods and Applications*. American Geophysical Union, Washington, D.C, pp. 313–338.
- Hanks, T.C., Bucknam, R.C., Lajoie, K.R., Wallace, R.E., 1984. Modification of wave-cut and faulting-controlled landforms. *Journal of Geophysical Research* 89 (B7), 5771–5790.
- Heimsath, A.M., Dietrich, W.E., Nishiizumi, K., Finkel, R.C., 1999. Cosmogenic nuclides, topography, and the spatial variation of soil depth. *Geomorphology* 27 (1–2), 151–172.
- Heimsath, A.M., Chappell, J., Spooner, N.A., Questiaux, D.G., 2002. Creeping soil. *Geology* 30, 111–114.
- Heimsath, A.M., Furbish, D.J., Dietrich, W.E., 2005. The illusion of diffusion: field evidence for depth-dependent sediment transport. *Geology* 33 (12), 949–952.
- Hudiberg, T., Law, B., Turner, D.P., Campbell, J., Donato, D., Duane, M., 2009. Carbon dynamics of Oregon and Northern California forests and potential land-based carbon storage. *Ecological applications* 19 (1), 163–180.
- Hughes, M., Almond, P., Roering, J., 2009. Increased sediment transport via bioturbation at the last glacial–interglacial transition. *Geology* 37 (10), 910–922.
- Jackson, R.B., Canadell, J., Ehleringer, J.R., Mooney, H.A., Sala, O.E., Schulze, E.D., 1996. *Oecologia* 108, 389–411.
- Johnson, D.L., 1990. Biomantle evolution and the redistribution of earth materials and artifacts. *Soil Science* 149, 84–102.
- Kaste, J.M., Heimsath, A.M., Bostick, B.C., 2007. Short-term soil mixing quantified with fallout radionuclides. *Geology* 35 (3), 243–246.
- Kirkby, M.J., 1971. Hillslope process–response models based on the continuity equation. Institute of British Geographers Special Publication 3, 15–30.
- Lehmkuhl, J.F., Kistler, K.D., Begley, J.S., 2006. Bushy-tailed woodrat abundance in dry forests of eastern Washington. *Journal of Mammalogy* 87 (2), 371–379.
- Lutz, H.J., 1960. Movement of rocks by uprooting of forest trees. *American Journal of Science* 258, 752–756.
- Lutz, H.J., Griswold, F.S., 1939. The influence of tree roots on soil morphology. *American Journal of Science* 237, 389–400.
- McDonald, E.V., Busacca, A.J., 1992. Late Quaternary stratigraphy of loess in the channelled scabland and Palouse regions of Washington State. *Quaternary Research* 38, 141–156.
- McKean, J.A., Dietrich, W.E., Finkel, R.C., Southon, J.R., Caffee, M.W., 1993. Quantification of soil production and downslope creep rates from cosmogenic ^{10}Be accumulations on a hillslope profile. *Geology* 21, 343–346.
- Mort, M., 2003. Tree-throw and its contribution to soil production in the Oregon Coast Range. M.S. thesis, University of Oregon, Eugene.
- Munsell, A.H., 1976. *Munsell Book of Color: Glossy Finish Collection, Removable Samples in Two Binders*. Munsell Color, Baltimore.
- Nash, D.B., 1980. Morphologic dating of degraded normal fault scarps. *Journal of Geology* 88, 353–360.
- Norton, D.A., 1989. Tree windthrow and forest soil turnover. *Canadian Journal of Forest Research* 19 (3), 386–389.
- O’Green, A.T., Busacca, A.J., 2001. Late Quaternary paleoenvironments of the Columbia Plateau, PNW U.S., from faunal borrows in paleosols. *Palaeogeography, Palaeoclimatology, Palaeoecology* 169, 23–37.
- Paton, T.R., Humphreys, G.S., Mitchell, P.B., 1995. *Soils: a New Global View*. UCL Press, London, 212 pp.
- Reimer, P.J., Baillie, M.G.L., Bard, E., Bayliss, A., Beck, J.W., Bertrand, C.J.H., Blackwell, P.G., Buck, C.E., Burr, G.S., Cutler, K.B., Damon, P.E., Edwards, R.L., Fairbanks, R.G., Friedrich, M., Guilderson, T.P., Hogg, A.G., Hughen, K.A., Kromer, B., McCormac, G., Manning, S., Ramsey, C.B., Reimer, R.W., Remmele, S., Southon, J.R., Stuiver, M., Talamo, S., Taylor, F.W., van der Plicht, J., Weyhenmeyer, C., 2004. IntCal04 terrestrial radiocarbon age calibration, 0–26 cal kyr BP. *Radiocarbon* 46 (3), 1029–1058.
- Reneau, S.L., Dietrich, W.E., 1991. Erosion rates in the southern Oregon Coast Range: evidence for an equilibrium between hillslope erosion and sediment yield. *Earth Surface Processes and Landforms* 16, 307–322.
- Roering, J.J., 2008. How well can hillslope models “explain” topography? Simulating soil transport and production with high-resolution topographic data. *GSA Bulletin* 120 (9/10), 1248–1262.
- Roering, J.J., Kirchner, J.W., Dietrich, W.E., 1999. Evidence for nonlinear, diffusive sediment transport on hillslopes and implications for landscape morphology. *Water Resources Research* 35, 853–870.
- Roering, J.J., Almond, P., Tonkin, P., McKean, J., 2002. Soil transport driven by biological processes over millennial time scales. *Geology* 30, 1115–1118.
- Roering, J.J., Schmidt, K.M., Stock, J.D., Dietrich, W.E., Montgomery, D., 2003. Shallow landsliding, root reinforcement, and the spatial distribution of trees in the Oregon Coast Range. *Canadian Geotechnical Journal* 40, 237–253.
- Roering, J.J., Almond, P., Tonkin, P., McKean, J., 2004a. Constraining climatic controls on hillslope dynamics using a coupled model for the transport of soil and tracers: application to loess-mantled hillslopes, South Island, New Zealand. *Journal of Geophysical Research* 109 (1), 1–19.
- Roering, J.J., Almond, P., Hughes, M.W., 2004b. Biological modulation of glacial–interglacial variations in soil transport and hillslope evolution. *Geological Society of America Abstracts with Programs* 36 (5), 386.
- Schaetzl, R.J., 1986. Complete soil profile inversion by tree uprooting. *Physical Geography* 7, 181–189.
- Schaetzl, R.J., Burns, S.F., Small, T.W., Johnson, D.L., 1990. Tree uprooting: review of types and patterns of soil disturbance. *Physical Geography* 11, 277–291.
- Schaller, M., Ehlers, T.A., Blum, J.D., Kallenberg, M.A., 2009. Quantifying glacial moraine age, erosion, and soil mixing with cosmogenic depth profiles. *Journal of Geophysical Research – Earth Surface* 114, F01012, doi:10.1029/2007JF000921.
- Schmidt, K.M., Roering, J.J., Stock, J.D., Dietrich, W.E., Montgomery, D., Schaub, T., 2001. The variability of root cohesion as an influence on shallow landslide susceptibility in the Oregon Coast Range. *Canadian Geotechnical Journal* 38 (5), 995–1024.
- Schulze, E.-D., Mooney, H.A., Sala, O.E., Jobbagy, E., Buchmann, N., Bauer, G., Canadell, J., Jackson, R.B., Loreti, J., Oosterheld, M., Ehleringer, J.R., 1996. *Oecologia* 108, 503–511.
- Small, T.W., Schaetzl, R.J., Brixie, J.M., 1990. Redistribution and mixing of soil gravels by tree uprooting. *Professional Geographer* 42, 445–457.
- Small, E.E., Anderson, R.S., Hancock, G.S., 1999. Estimates of the rate of regolith production using ^{10}Be and ^{26}Al from an alpine hillslope. *Geomorphology* 27, 131–150.
- Stokes, A., 2002. Biomechanics of tree root anchorage. In: Waisel, Y., Kafkafi, U. (Eds.), *Plant Roots, the Hidden Half*. Marcel Dekker, Inc., New York.
- Sweeney, M.R., 2004. Sedimentology, Paleoclimatology, and Geomorphology of a Late Pleistocene–Holocene Paired Eolian System, Columbia Plateau. PhD Dissertation, Washington State University, Pullman, WA.
- Sweeney, M.R., Gaylord, D.R., Busacca, A.J., Richardson, C.A., Reyerson, P., Blinnikov, M., 2006. A new luminescence chronology and paleoecologic history of Holocene loess, Pacific Northwest, USA. *Geological Society of America Abstracts with Programs* 38 (7), 72.
- Tucker, G.E., Bras, R.L., 1998. Hillslope processes, drainage density, and landscape morphology. *Water Resources Research* 34, 2751–2764.
- Tyler, A.N., Carter, S., Davidson, D.A., Long, D.J., Tipping, R., 2001. The extent and significance of bioturbation on ^{137}Cs distributions in upland soils. *Catena* 43, 81–99.
- Walling, D.E., He, Q., 1999. Improved models for estimating soil erosion rates from cesium-137 measurements. *Journal of Environmental Quality* 28, 611–622.
- Walther, S.C., 2006. Quantifying Biogenic Sediment Transport on a Forested, Loess-Mantled Hillslope in the Blue Mountains, Eastern Washington. MS Thesis, University of Oregon, Eugene, OR.
- Whitlock, C., Sarna-Wojcicki, A.M., Bartlein, P.J., Nickman, R.J., 2000. Environmental history and tephrostratigraphy at Carp Lake, southwestern Columbia Basin, Washington, USA. *Palaeogeography, Palaeoclimatology, Palaeoecology* 155, 7–29.
- Yoo, K., Mudd, S.M., 2008. Discrepancy between mineral residence time and soil age: implications for the interpretation of chemical weathering rates. *Geology* 36 (1), 35–38.
- Yoo, K., Amundson, R., Heimsath, A., Dietrich, W.E., 2005. Process-based model linking pocket gopher (*Thomomys bottae*) activity to sediment transport and soil thickness. *Geology* 33 (11), 917–920.